JOURNAL OF BIOMOLECULAR STRUCTURE AND DYNAMICS
2020, VOL. 38, NO. 6, 1659–1669
https://doi.org/10.1080/07391102.2019.1614998



# Molecular simulations of fluconazole-mediated inhibition of sterol biosynthesis

Tayane Honorato Siqueira and Leandro Martínez

Institute of Chemistry and Center for Computing in Engineering & Sciences, University of Campinas, Campinas, Brazil

Communicated by Ramaswamy H. Sarma

**ABSTRACT**

Invasive opportunistic fungal infections and antifungal drug resistance prompt the investigation of the underlying molecular mechanisms of the inhibition of the triazole drugs. The target of triazoles is the product of the ERG11 gene, the cytochrome P450 sterol 14α-demethylase (CYP51), which is part of the ergosterol biosynthetic pathway. In this study, molecular dynamics (MD) simulations were performed to reveal the mechanisms of fluconazole inhibitory activities in orthologs of CYP51 present in humans (Hs), and in *Mycobacterium tuberculosis* (Mt), *Candida albicans* (Ca) and *Candida glabrata* (Cg). The conformational diversity of the BC loop in the CYP51-Hs and CYP51-Mt structures alter the catalytic site of these enzymes when compared to the fungal CYPs, resulting in greater conformational variability of the inhibitor. Overall interaction energies are consistent with the observed affinities, but are the result of the competitive interactions of the ligand with the protein residues, the HEME group and water molecules. Specifically, protein–fluconazole interactions are more effective in CYP51-Mt due to polar interactions with the Arg96 residue. These interactions are, however, substituted in fungal enzymes by ligand–HEME interactions, which compensate for the loss of the polar bond and result in a more energetically favored binding. Therefore, the development of ligand with increased specificity to fungal enzymes should focus on the strengthening polar ligand–HEME interactions, while larger hydrophobic ligands are probably best suited to target mycobacterial and human enzymes. These differences and other ligand-binding site-specific interactions are presented and can inspire the design of new inhibitors with greater ortholog specificity.

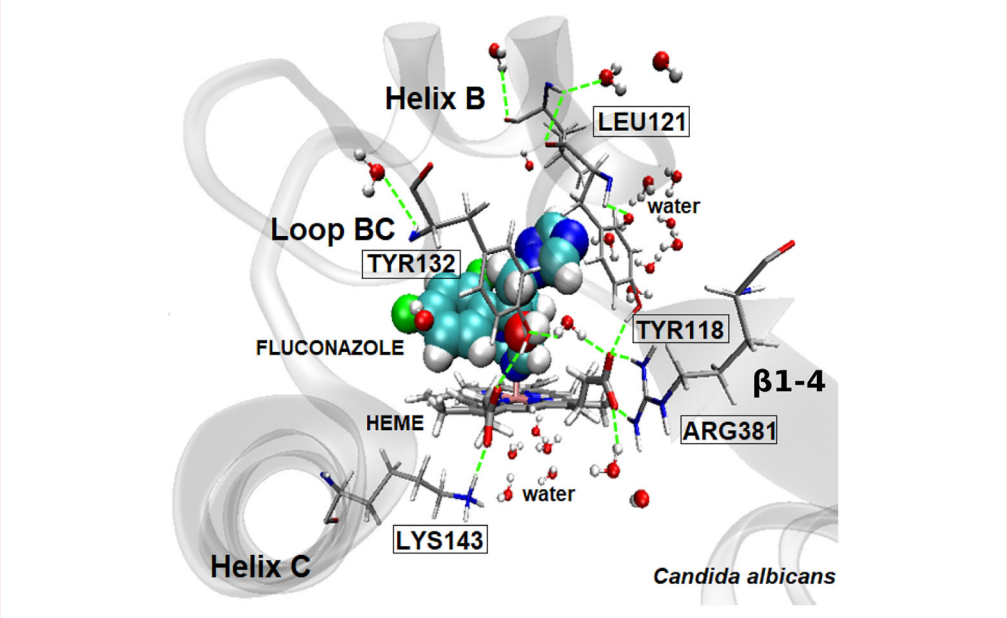


Fluconazole displays greater affinity to fungal CYP51 enzymes because it forms polar interactions with the HEME carboxylates which are not stable in human or mycobacterial orthologs.

**Abbreviations:** CYP51: cytochrome P450 sterol 14α-demethylase; MD: molecular dynamics; PDB: Protein Data Bank; RMSF: root mean square fluctuations

**ARTICLE HISTORY**
Received 26 December 2018
Accepted 29 April 2019

**KEYWORDS**
Fluconazole; selectivity; molecular dynamics simulations; *Candida*; cytochrome P450

CONTACT Leandro Martínez leandro@iqm.unicamp.br

Supplemental data for this article is available online at https://doi.org/10.1080/07391102.2019.1614998.

## 1. Introduction

Pathogenic fungi cause around 11.5 million infections and superficial mycoses worldwide every year (Bongomin, Gago, Oladele, & Denning, 2017). The mortality caused by fungi diseases is of 1.5 million people per year, comparable to that of tuberculosis and three times greater than that of malaria (Bongomin et al., 2017; Brown, Denning, & Levitz, 2012). Fungal infections are considered neglected diseases, being harmful to people with immunosuppression or overall poor health conditions (Bongomin et al., 2017; Brown et al., 2012).

The resistance of fungi to current drugs demands the development of new classes of antifungal compounds. Antifungal drugs are relatively difficult to develop compared to the antibacterial drugs due to the eukaryotic nature of the cells. In particular, antifungal medicines based on the triazolic class, as fluconazole (considered by the World Health Organization an Essential Medicine), are progressively found to be insufficient to treat many infections. Therefore, new drugs must be developed, urging the understanding of the molecular basis of fluconazole affinity and specificity.

The target molecule of fluconazole is the product of the ERG11 gene, the cytochrome P450 sterol 14α-demethylase (CYP51, $P450_{14\text{-}DM}$). The CYP51 enzyme converts lanosterol to ergosterol, thus being part of the biosynthetic route of a major component of the fungal cellular membrane (Balding et al., 2008). The inhibition of the ergosterol synthesis retards the development of the fungal cells by the accumulation of toxic steroids such as methylated sterol (Lupetti, Danesi, Campa, Del Tacca, & Kelly, 2002; Marichal et al., 1999; White, Marr, & Bowden, 1998), perturbing the membrane integrity, fluidity and permeability (Shapiro, Robbins, & Cowen, 2011). Fluconazole acts as a competitive inhibitor to CYP51 and is currently efficient to treat many pathogenic fungi, including *Candida albicans* and *Candida glabrata* (Marichal et al., 1999).

*Candida* sp. are the most common fungal etiological agents of life-threatening invasive infections. Even though *C. albicans* is still considered the major pathogen associated with candidemia, the incidence of infections due to non-albicans species such as *C. glabrata* is increasing and may display resistance to some antifungal agents. In particular, resistance to fluconazole is frequent. This is a major problem as fluconazole is the most commonly used antifungal agent for prophylaxis and treatment of *Candida* infections in many parts of the world (Bongomin et al., 2017; Castanheira, Messer, Jones, Farrell, & Pfaller, 2014; Pfaller et al., 2014).

Fluconazole binds the human CYP51 with low affinity ($k_d$=30.5 μM; Warrilow, Parker, Kelly, & Kelly, 2013) and is also known to display some antimycobacterial activity ($k_d$=10 μM; Bellamine, Mangla, Nes, & Waterman, 1999; McLean et al., 2006). Its affinity to fungal CYP51 targets is much higher, displaying nano-molar dissociation constants on *C. albicans* and *glabrata* fungal strains ($k_d$=56 nM; Warrilow et al., 2013; Park et al., 2011). The crystal structures of CYP51 from *Mycobacterium tuberculosis* bound to azole inhibitors is known since 2001 (Podust, Poulos, & Waterman, 2001) and the structure of ketoconazole bound to the human ortholog was obtained in 2010 (N. Strushkevich, Usanov, & Park, 2010). On the other side, the structure of Candida CYP51s complexed with a tetrazole, oteseconazole, was obtained only recently (T. Y. Hargrove et al., 2017). These structures are fundamental for the understanding and design of new inhibitors of the fungal variants. Modeling approaches have been used recently to suggest new pyrazole analogs based on a CYP51-Ca homology model (Doğan et al., 2017; Jacob, Ganguly, Kumar, Poddar, & Kumar, 2017). Also, molecular simulations have been used to rationalize the affinities of various inhibitors towards CYP51 orthologs and (Gao, Cui, & Wu, 2018) and to understand the role of mutations in the stability and binding affinity of the enzymes (Keighobadi et al., 2018; Vijayakumar & Das, 2019). However, we are not aware of any study aiming the understanding of the greatest affinity of fluconazole to fungal enzymes relative to mycobacterial and human orthologs. A recent overview of the modeling strategies used for ligand design for the P450s can be found in (Kontoyianni & Lacy, 2018).

In this work, we performed molecular dynamics simulations (MD) to characterize the structural and dynamical properties of the interactions of fluconazole with different fungi, mycobacterial and human CYP51 enzymes, for which structural data are available (T. Y. Hargrove et al., 2017; Podust et al., 2001; N. Strushkevich et al., 2010). The comparative analysis of the enzymes and the MD simulations allowed the identification of structural, dynamical and energetic fingerprints differentiating the interactions of fluconazole with each CYP51. Estimated interaction strengths based on interaction energies and docking scores are consistent with the experimentally observed affinities and can be rationalized in terms of the interactions of the ligand with the protein, the HEME group and the solvent. The particularities of the interactions of fluconazole with each of the targets can be associated with structural differences observed in the crystallographic structures. These studies provide insights for the development of ligands with greater affinity and specificity towards mycobacterial and fungal targets.

## 2. Materials and methods

### 2.1. Structure preparation

This study evaluated the inhibitory activity of fluconazole on Sterol 14-α-demethylase (CYP51) orthologs. Comparative structural analyses of the P450 CYP51 enzymes *C. albicans* (CYP51-Ca), *C. glabrata* (CYP51-Cg), *M. tuberculosis* (CYP51-Mt) and *Homo sapiens* (CYP51-Hs) complexed to the drug fluconazole were performed by molecular dynamics (MD) simulations. We used the recently obtained fungal CYP51 crystallographic structures of *C. albicans* (CYP51-Ca, PDB id. 5TZ1; resolution: 2.0Å) in complex with newest tetrazole-based drug candidates (oteseconazole; T. Y. Hargrove et al., 2017), of *C. glabrata* (CYP51-Cg, PDB id. 5JLC; resolution: 2.4Å) in complex with itraconazole (Sagatova, Keniya, Wilson, Monk, & Tyndall, 2015). The human ortholog was obtained in complex with ketoconazole (PDB id. 3LD6; resolution 2.8Å; N. V. Strushkevich, Harnastai, & Usanov, 2010).

The structure of CYP51-Mt bound to fluconazole (PDB id. 1EA1; resolution: 2.21Å; Podust et al., 2001) was used as a reference structure because it is co-crystallized with the

inhibitor of interest. The coordinates of the fluconazole ligand present in this structure were initially transported to *C. albicans* (T. Y. Hargrove et al., 2017), *C. glabrata* (Sagatova et al., 2015) and *H. sapiens* (N. V. Strushkevich et al., 2010) to generate the initial molecular model of their respective complexes. As we will show, the fluconazole molecule relaxed in all models, assuming distinct and variable conformations during the MD simulations, providing a broader view of the ligand binding structure and dynamics. The fluconazole conformations observed in the MD simulations were also consistent with docking poses obtained in this study (see Sections 3 and 4).

Fungal CYP51s contain N-terminal helical transmembrane domains that are not present in CYP51-Mt or CYP51-Hs. In our simulations, we disregarded the presence of the transmembrane helix determined in the structure of CYP51-Cg (PDB id 5JLC). The absence of the transmembrane domain membrane is justified in the present work because the fluconazole binding site is relatively distant from it.

### 2.2. Molecular dynamics protocol

Molecular dynamics (MD) simulations were performed using the NAMD program (Kalé et al., 1999), with the CHARMM36 force-field with CMAP corrections for the protein and the HEME group (Huang & MacKerell, 2013; MacKerell et al., 1998; Vanommeslaeghe, Raman, & MacKerell, 2012), and the TIP3P model for water (Jorgensen, Chandrasekhar, Madura, Impey, & Klein, 1983). The CHARMM General Force-Field (v3.1) obtained from the cgenff.paramchem.org server (v1.0) (Vanommeslaeghe et al., 2010, 2012) was used for atom types and partial atomic charges for the ligand fluconazole by analogy. Missing bond, angle and dihedral parameters, and the partial charges of all atoms of fluconazole were optimized using the Force Field Toolkit (ffTK) – plugin of the VMD program (Mayne, Saam, Schulten, Tajkhorshid, & Gumbart, 2013; see Tables S1, S2, and S3 in Supplemental Material for a complete list of parameters). All hydrogen atoms of the enzyme, HEME group and fluconazole ligands were added using the psfgen program of the NAMD package. The protonation states of the histidines were determined using the online H++ server (Gordon et al., 2005).

All systems were solvated with a minimum 15 Å shell of water using the VMD solvate plugin. To neutralize the system and mimic a physiological ionic strength, $Na^+$ ions and $Cl^-$ ions were added using the autoionize plugin of VMD (Humphrey, Dalke, & Schulten, 1996a), at a concentration of 0.15 M. Langevin piston and thermostat were used to maintain the pressure at 1 atm and the temperature at 310 K. Therefore, the ensembles simulated were isothermal–isobaric. Periodic boundary conditions were used. The short- and long-range interactions were calculated at each 1 and 2 integration steps, respectively. Long-range electrostatic interactions were computed with the Particle-Mesh-Ewald summation methodology (Essmann et al., 1995). The Velocity-Verlet algorithm (Swope, Andersen, Berens, & Wilson, 1982) was used with a 2 fs simulation time-step.

For equilibration, we performed the following sequential steps of minimization (with the Conjugate Gradient algorithm) and MD simulations: (i) 10,000 minimization steps with restrictions on all atoms of the protein structure, the HEME and fluconazole to allow the relaxation of the solvent, followed by 200 ps MD; (ii) 500 steps of minimization and 200 ps MD with restrictions on the Cα atoms of the protein only; (iii) 2.2 ns MD with no restrictions. Finally, four independent production MD simulations of 50 ns were performed for each system under study.

The sequence alignment of Figure S1 in the Supplemental Material was generated with the Clustal-Omega program (Sievers et al., 2011), and secondary structure information was added to this alignment with the help of the web server ENDscript (Robert & Gouet, 2014). The distribution the distances and potential energies between fluconazole and key residue of the catalytic site as a function of time were calculated using the MDanalysis suite developed in our group (L. Martínez, 2017). Analysis of the mobility and structural fluctuation as a function of time such root mean square deviation (RMSD) and root mean square fluctuations (RMSF) were calculated using MDLovoFit (L. Martínez, 2015). VMD (Humphrey, Dalke, & Schulten, 1996b; Schrödinger, 2015) and Pymol (Schrödinger, 2015) were used to visualize the MD and produce figures.

### 2.3. Molecular docking protocol

Molecular docking was performed using the DockThor program, an online server designed to deal with highly flexible ligands using a multiple-solution steady-state genetic algorithm. The scoring function is based on the MMFF94S classical force field (de Magalhães, Barbosa, & Dardenne, 2004; de Magalhães, Almeida, Barbosa, & Dardenne, 2014). A $10 \times 10 \times 10$ Å was used, binned in 0.25 Å intervals. Comparative molecular docking analysis was performed to understand the change in binding modes of the CYP51 orthologs. The results were analyzed interactively in the DockThor server site (https://dockthor.lncc.br/v2/).

## 3. Results

### 3.1. Comparative structural analysis of sterol 14-α-demethylase orthologs

We performed the structural alignment of the four CYP51 orthologs and obtained the residue correspondence and structural variability. The sequence identity of CYP51-Ca with its ortholog CYP51-Cg is of 63%, and the root mean square deviation (RMSD) of their Cα atoms is 0.91 Å. The sequence identity of CYP51-Ca with CYP51-Mt is of only 21% and with CYP51-Hs is 39%. The RMSD of Cα atoms between CYP51-Ca and CYP51-Mt is of 1.98 Å, and that between CYP51-Ca and CYP51-Hs is 1.38 Å. The Cα RMSDs, which are always smaller than 2 Å, demonstrate a significant structural similarity between the orthologs.

The catalytic sites of the enzymes are formed by a series of invariant residues conferring to the P450, family 51,

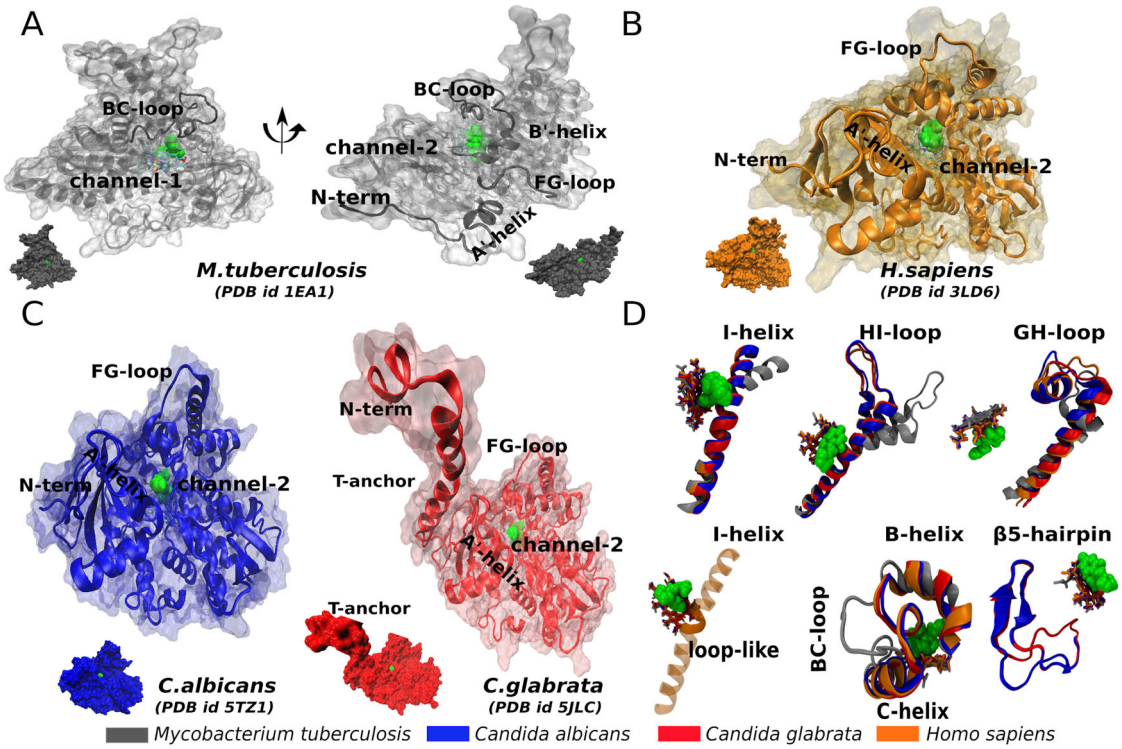


**Figure 1.** Comparative analysis of the CYP51 structures of this study. (A) In CYP51-Mt (PDB id 1EA1), two channels connect the binding site with the solvent: Channel 2, which is common to all CYP51s, and Channel 1, which is specific of CYP51-Mt. Channel 1 exists in CYP51-Mt because of the greater length and flexibility of the BC-loop. (B, C) The human CYP51 (PDB id. 3LD6) and fungal structures CYP51-Ca (PDB id 5TZ1), CYP51-Cg (PDB id 5JLC) display Channel 2 in common with CYP51-Mt. (C) CYP51-Cg has an additional transmembrane helix (T-anchor). (D) The structural superposition of the four CYP51 orthologs indicates the regions of greater variability: the I-helix, the HI-loop and H-helix, and the GH-loop and G-helix are displaced in CYP51-Mt relative to fungal and human enzymes; there is a loop-like segment in the middle portion of the I-helix in CYP51-Hs; the longer BC-loop of CYP51-Mt leads to the aperture of Channel 1; the β5-hairpin, which is a phylum-specific segment of fungal CYP51 enzymes. The ligand is shown in vdW representation in green and HEME cofactor is shown as sticks.

characteristic sequence signatures (a detailed sequence alignment is shown in Supplemental Material, Figure S1). These residues are believed to be minimum requirements for CYP51 catalytic activity (T. Hargrove, Wawrzak, & Lepesheva, 2017; Lepesheva & Waterman, 2007, 2011).

The most conserved structural region between the four orthologs studied here is the Heme-bulge. It contains the F-G-x-G-R-H-R-C-x-G motif before helix L, and its cysteine residue is highly conserved within the family 51 of the cytochrome P450. In helix K, the motif K-E-T-L-R is found. Helix B′ contains the sequence known as signature I (A-Y-x-x-x-x-T-P-x-F-G), and the central part of helix I contains the signature II (G-x-H-T-S-x-x-T-x-x-W).

The structural differences between the orthologs involve important regions associated with ligand binding and release from the catalytic pocket. Two channels connect the binding pocket with the solvent in CYP51-Mt, as shown in Figure 1(A). Channel 1 is observed in CYP51-Mt only, between helix B′ and loop BC. Channel 2 exists in all four CYPs and is formed by the C-terminal region of helix F, the N-terminal part of helix G and the FG-loop, as shown in Figure 1(A–C) (Choi & Roush, 2016; Podust et al., 2001; Sheng et al., 2010).

Additional filo-specific structural differences might be important for the development of inhibitory compounds of high specificity: (i) The presence of the transmembrane region (T-anchor) in fungal enzymes (Figure 1(C)) and mammal CYP51s, which is absent in mycobacterial strains; (ii) The difference in the structure and position of helices H and I (Figure 1(D)). These helices are displaced in CYP51-Mt relative to their positions in other CYPs. As shown in Figure 1(D), the N-terminal region of helix I displays a tilt in CYP51-Mt, associated to a significant variability of the HI-loop and of the helices G and H. (iii) Fungal and human CYPs display a BC-loop which is shorter than that of CYP51-Mt. This leads the CYPs to assume a closed loop conformation, as shown in Figure 1(D) (lower figure). The longer sequence and open conformation of the BC-loop in CYP51-Mt lead to a significantly greater solvent access to the active site (Choi & Roush, 2016; T. Y. Hargrove et al., 2017; Podust et al., 2001). (iv) The human ortholog displays a discontinuity in the I-helix within residues Gly312 and Ser316, providing greater flexibility to this region (T. Y. Hargrove et al., 2017). (v) Fungal CYP51s are the only enzymes of the P450 cytochrome displaying the β5-hairpin, shown in Figure 1(D) (refer to Supplemental Material, Figure S1 for a sequence alignment of the four orthologs in this region). This hairpin is composed of a sequence insertion between the meander region and the Heme-bulge, and displays functional importance. The fungal CYP51s depend on the cytochrome P450 reductase NADPH (CPR) (Kenaan, Zhang, Shea, & Hollenberg, 2011), an electron-donor cofactor, and the β5-hairpin is believed to mediate this interaction (T. Y. Hargrove et al., 2017; T. Y. Hargrove, Wawrzak, Lamb, Guengerich, & Lepesheva, 2015; Kenaan et al., 2011; Podust et al., 2001).

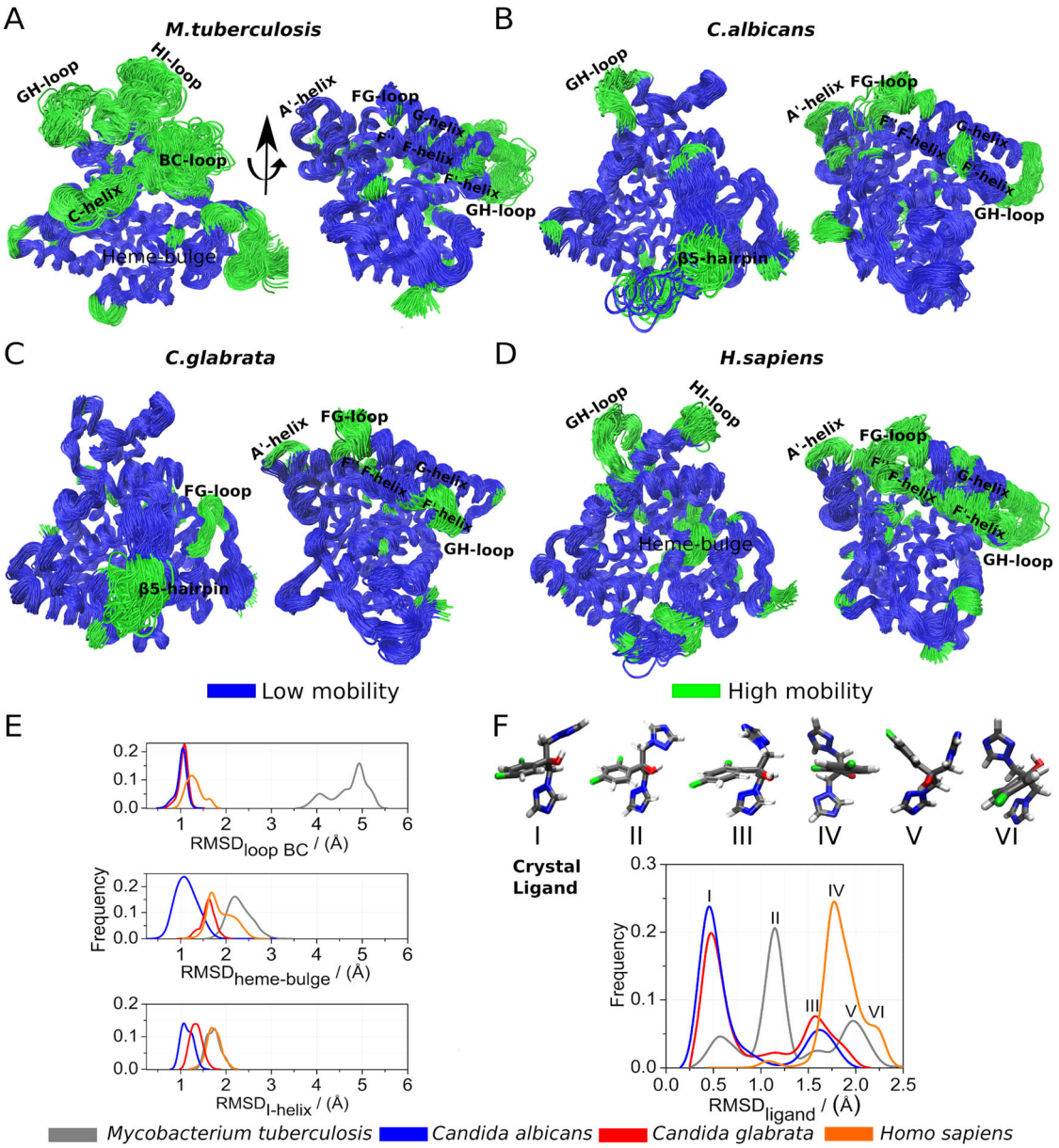


Figure 2. Structural fluctuations of CYP51 structures. (A) CYP51-Mt, (B) CYP51-Ca, (C) CYP51-Cg and (D) CYP51-Hs. Regions of lower flexibility are shown in blue, and regions of higher flexibility are shown in green. (E) RMSDs of the BC-loop, the HEME-bulge and the I-helix, showing the greater structural fluctuations of these regions in CYP51-Mt and CYP51-Hs relative to fungal orthologs. (F) Conformations of the ligand in the binding pocket: six different conformations are observed, being the crystallographic one predominant in fungal enzymes, while the most frequent conformation in CYP51-Mt differs from the crystallographic structure by a rotation of one of the triazole rings. The most frequent conformation in CYP51-Hs differs from the crystallographic structure by a rotation of the triazole and 2,4-difluorophenyl rings and by the inclination of the molecule in relation to the Heme plane.

### 3.2. Structural fluctuations of the CYP51 enzymes and interactions with fluconazole

Molecular dynamics simulations were performed for the four orthologs CYP51-Ca, CYP51-Cg, CYP51-Hs and CYP51-Mt, to evaluate the most important fluctuations relative to the crystallographic structures. The structural variability was characterized by computing the RMSD of the structures using the MDLovoFit software (Leandro Martínez, 2015). This software performs a robust structural alignment in which the most conserved regions are automatically identified. For all enzymes, at least 80% of the Cα atoms could be aligned to the initial structure of the simulations to RMSDs smaller than 1 Å. This indicates that, in general, the structures are stable in the time-scale of the simulations.

Figure 2(A–D) displays the superposition of the frames of the simulations, after alignment. The 80% least mobile residues are shown in blue and the 20% most flexible residues are shown in green. The greater structural variability of CYP51-Mt is evident, particularly at the C-helix, the HI-, GH- and BC-loops, and at the N-terminal residues, as shown in Figure 2(A). Figure 2(E) shows that, specifically for the BC-loop, there is a significant flexibility difference between CYP51-Mt and the other orthologs. The shorter loop in fungal and human CYP51s result in reduced flexibility, resembling that of the core regions of the protein. The BC-loop in CYP51-Mt, on the other side, fluctuates quite significantly displaying deviations of the order of 4–5 Å from the crystallographic conformation.

The most mobile regions of the fungal enzymes are the FG-loop and the β5-hairpin, as shown in Figure 2(B,C). This hairpin, as pointed before, is exclusive of fungal CYP51s. The human ortholog displays greater flexibility than the other CYP51s in helices A′, B′, F, F′, F″, and G, in the FG-loop. The increased flexibility of the FG-loop and F-helices can be noticed in Figure 2(D).

These simulations show, therefore, that there is a significant correlation between the regions of low structural similarity between CYP51 enzymes and their structural flexibility. The structural difference shown in Figure 1(D) for the BC-loop is associated with this loop being highly flexible in CYP51-Mt. This structural and dynamical peculiarity of the mycobacterial enzyme leads to the aperture of Channel 1 of possible ligand binding and release (Figure 1(D)).

The BC-loop is close to the binding pocket, and its flexibility is reflected by the dynamics of fluconazole. Also close to the binding pocket we observe the discontinuity of the I-helix in CYP51-Hs. The fungal BC-loops are the most rigid and, as shown in Figure 2(F), the structural deviations of the ligand from the crystallographic pose, in the binding pocket of fungal CYP51s, are smaller than in CYP51-Mt and CYP51-Hs. These structural differences cause conformational variations in the ligand binding modes. Fluconazole is able to assume six different conformations, as judged by their RMSDs relative to the crystallographic conformation, as shown in Figure 2(F). Conformation I is the crystallographic one, and completely preponderant in the simulations of CYP51-Ca and CYP51-Cg. The most frequent conformation in CYP51-Mt differs in about 1.2Å RMSD from the conformation of fungal enzymes, but the crystallographic conformation is also present. In the human CYP51, on the other side, fluconazole assumes preponderant conformations which differ as much as 2.2Å from the crystallographic fluconazole binding mode. Conformations I and II differ by rotations of one of the triazole rings, while conformation III–VI result from the combined rotations of the triazole and difluorophenyl rings leading to different conformers. Conformations V and VI, which are the most frequent for CYP51-Hs, are characterized by a tilt of the molecule in the active site. We will show that these conformational differences affect the estimated affinities of fluconazole to each ortholog.

### 3.3. Inhibition of the catalytic activity of CYP51 orthologs

The fluconazole molecule inhibits CYP51 enzymes by forming a coordinate covalent bond to the HEME iron. However, its specificity depends on the interactions of the triazole and difluorophenyl rings with the residues of the active site, which are shown in Figure 3(A). We computed the fraction of the simulation time during which these residues remained in contact with the triazole or difluorophenyl rings. The residues were considered in contact if the minimum distance between any of their atoms was smaller than 4 Å. Seven residues were found to be in contact with the ligand in at least of one the structures and displayed different interactions in each ortholog. The percentage of time of these interactions in the simulations is shown in Figure 3(B).

The triazole ring of fluconazole points to the region containing Channel 1 (helix B′ and I, sheets β1-4 and β4-1 and the loop connecting helix K and sheets β1-4; Figure 1(B)). It forms a T-shaped stacking with the phenol ring of Tyr in position 76 (numbering for CYP51-Mt).

The interactions between fluconazole and the binding site which are mostly different between the human ortholog and the fungal enzymes are those of the F152 (in CYP51-Hs) residue, which is substituted by L139 in CYP51-Ca and L148 in CYP51-Cg. The fluconazole–F152 interaction is, nevertheless, not stabilized by direct interactions. Instead, The F152 residue forms a stacking interaction with Y145, which by its turn forms a hydrogen bond with one of the Heme carboxylates (Figure 3(E)). This hydrophobic packing is not possible in the other orthologs, either because the stacking interaction is not possible in fungal variants (as the Phe residue is substituted by Leu residues) or because the residue is charged (R96) in CYP51-Mt.

At the same time, there are two interactions that are fundamentally different between the fungal and mycobacterial enzymes: the interactions with the aromatic residue in position 89 (F89 in CYP51-Mt, and Y132/Y141 in CYP51-Ca and -Cg, respectively), and the interactions with R96 (CYP51-Mt) and hydrophobic residues in the corresponding position in fungal enzymes (L139/L148 in CYP51-Ca and -Cg, respectively). The interaction of fluconazole with Y132/Y141 of fungal enzymes is very stable, as shown in Figure 3(B). At the same time, the corresponding CYP51-Mt residue, F89, was not observed to contact the ligand. Fluconazole interacts persistently, however, with R96 of CYP51-Mt, in the same position of the F152 residue of CYP51-Hs which was discussed above. This polar interaction is crucial for the differential binding modes relative to fungal enzymes because the residues in the corresponding positions in CYP51-Ca and CYP51-Cg are leucines, thus hydrophobic counterparts. The leucine residues in positions L139 and L148 were observed to be in contact with the ligand, but only for about 10% of the simulation time.

No hydrogen bond was found between the ligand and the active site residues in the orthologs studied here. However, some polar interactions and hydrogen bonds occur between the active site residues and the propionate groups of the HEME leading to differences in the active site arrangement. Specifically, Tyr118 (from CYP51-Ca ring A) and Tyr132 (CYP-51 ring D) which are substituted in CYP51-Cg by Tyr127 and Tyr141 and in CYP51-Mt by Tyr76 and Arg96 form residue–HEME polar interactions. As shown in the first panel of Figure 3(C), the Tyr76/118/127/131 polar hydrogens interact with the HEME propionate group at a distance of about 2.9 Å. This interaction is eventually lost in the human ortholog. The Tyr132 residue from CYP51-Ca forms a hydrogen bond with the propionate group of the HEME which distinguishes its binding mode from that of CYP51-Cg. The corresponding residue in CYP51-Mt is F89, which is not observed to contact either the ligand or the HEME group but, in the

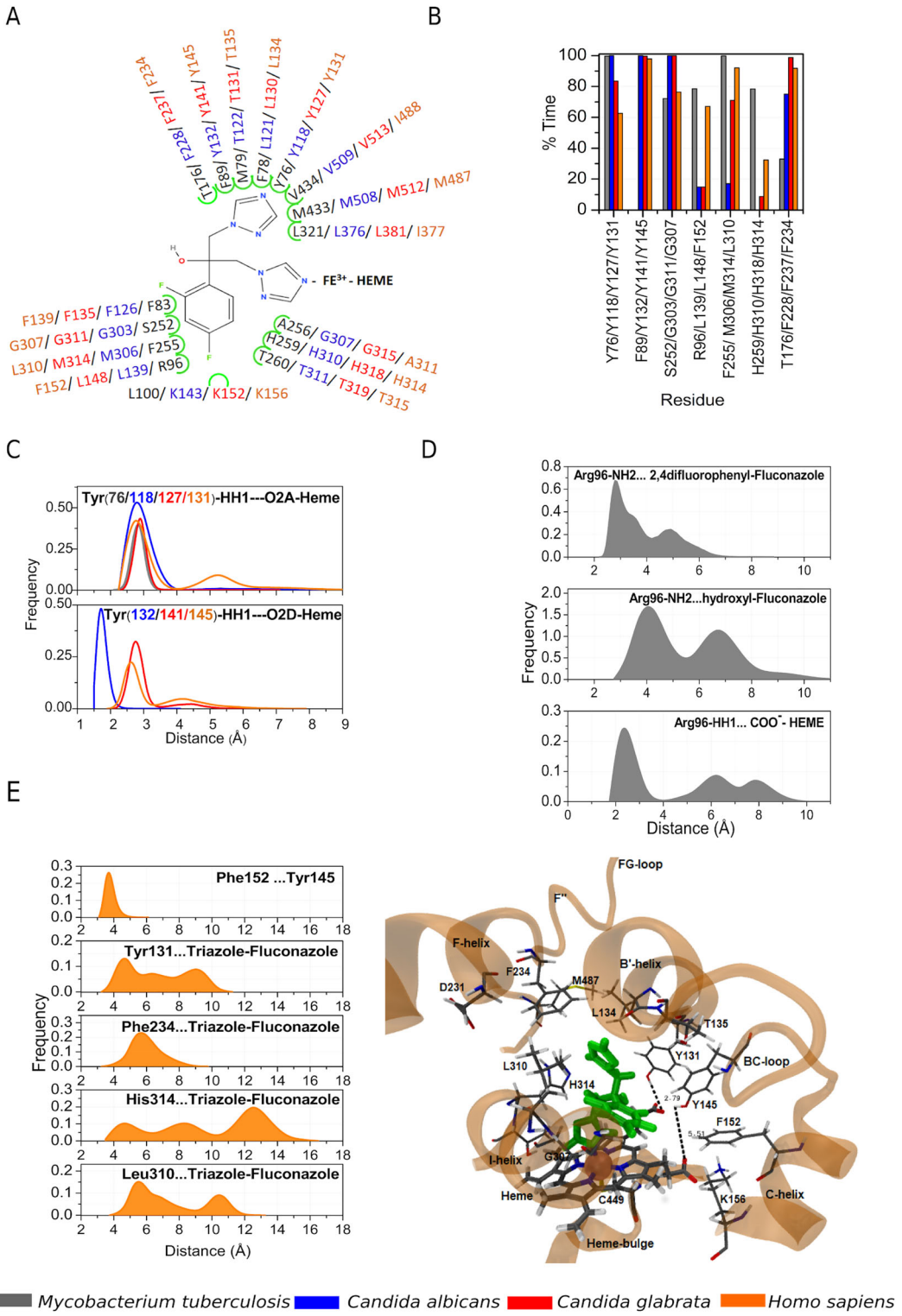


**Figure 3.** Active site residues and their interactions with fluconazole. (A) Residues belonging to the active site according to the crystallographic models. One important difference between fungal enzymes and the Mt and Hs orthologs occurs in the Arg96/Leu139/Leu148/Phe152 position. (B) Residues in contact with fluconazole during the simulations and displayed different interaction profiles with the ligand. (C) Distances of Tyr76/118/127/131 and Phe89/Tyr132/141/145 to carboxylate atoms of the HEME groups, which compete with the polar interactions with the ligand. (D) Interactions of Arg96 of CYP51-Mt with the ligand and with HEME carboxylates. These polar interactions are unique to the mycobacterial enzyme. (E) Binding site interactions in CYP51-Hs: a persistent interaction occurs between the Tyr145 and Phe152 residues; and residues Tyr131, Phe234, His314 and Leu310 form sporadic but important interactions with fluconazole.

human ortholog, the corresponding Tyr145 interacts with the ligand as in CYP51-Cg.

Finally, the Arg96 residue of CYP51-Mt, which is the most important difference between the four enzymes, results to be quite dynamic. It forms strong polar interactions with the difluorophenyl group of the ligand (Figure 3(D)), with the hydroxyl group of fluconazole, and also forms sporadic hydrogen bonds with the propionate HEME groups. This arginine residue is localized in Helix C, quite near the BC-loop. This loop is recognized here to be one of the most

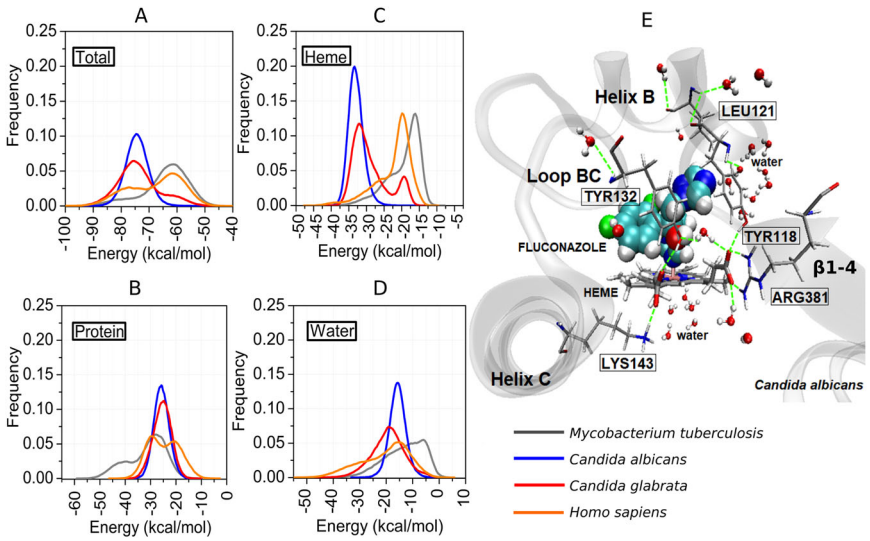


**Figure 4.** Interaction energies between fluconazole and the components of the systems: (A) total ligand–environment interactions; (B) ligand–protein interactions; (C) ligand–HEME interactions; (D) ligand–water interactions. (E) Representation of the binding site of CYP51-Ca displaying the penetration of water molecules in the active site in the region close to the BC-loop, which compensates partially the weaker ligand–protein interactions relative to CYP51-Mt and CYP51-Hs, but lead to binding destabilization.

mobile regions of CYP51-Mt, resulting in the observed dynamical behavior of the R96 residue. Therefore, the presence of a polar residue where fungal enzymes exhibit a hydrophobic counterpart leads to higher flexibility in the active site, with additional polar interactions.

In summary, the analysis of specific interactions of binding site residues with the ligand indicates that additional ligand–protein interactions are present in the CYP51-Hs and CYP51-Mt orthologs. This is apparently counterintuitive, as the affinity of fluconazole to fungal enzymes is greater, such that one could expect to find increased protein–ligand interactions in these proteins instead. However, as we will show, important ligand–HEME interactions are determinant for the ligand binding affinities. The additional protein–ligand interactions in the human and mycobacterial enzymes, rather than contributing to increasing the binding affinity, result from increased active site flexibility and occur at the expense of the interactions of the ligand with the HEME. These differences in interaction energies and flexibilities can be associated with the differential affinities observed experimentally, as we will discuss.

### 3.4. Interaction energies between fluconazole and CYP51 orthologs

The non-bonded interaction energies between the ligand and the environment, computed from the simulations, are more favorable for fungal enzymes than for CYP51-Mt and CYP51-Hs, as shown in Figure 4(A) and Table 1. The total interaction energies peak at about −75 kcal/mol for fungal enzymes and at about −60 kcal/mol for human and mycobacterial orthologs. The distributions of the energies indicate that there are two binding modes and that fluconazole conformations in CYP51-Cg (red), CYP51-Mt (black) and CYP51-Hs (orange) populate both, although with different relative probabilities. In CYP51-Ca (blue), on the other side, fluconazole populates only the low-energy binding mode.

Interestingly, protein–ligand interactions are more favorable in CYP51-Mt, as shown in Figure 4(B). This is a consequence of the interactions of the ligand with polar residues that are not present in fungal enzymes, specifically the R96. Fluconazole in CYP51-Mt interacts with the protein residues alternating two binding modes, a low-energy one, and a high-energy binding mode that mimics its interactions with the fungal and human enzymes. The low-energy ligand–protein interactions peak at about −42 kcal/mol, and in the high-energy mode they peak at about −25 kcal/mol, as shown in Figure 4(B). Thus, the binding modes differ in about 17 kcal/mol from the point of view of protein–ligand interactions. The interactions energies of the human ortholog with the ligand are, on average, similar to those of the fungal enzymes. However, the binding modes are not the same, and this can be inferred from the interaction energy profile (Figure 4(B)): for the human ortholog, two binding modes compete with each other with ligand–protein interaction energies of about −30 and −20 kcal/mol, while for fungal enzymes, a single binding mode with energies of −25 kcal/mol is observed.

Therefore, for different structural reasons, the binding of fluconazole to the human or mycobacterial orthologs is more variable than to fungal enzymes. In both cases, the ligand loses interactions with the HEME, as shown in Figure 4(C). Again, two binding modes are observed: a low energy binding mode peaking at about −27 kcal/mol and a high energy binding mode peaking at roughly −20 kcal/mol. The ligands in CYP51-Mt and CYP51-Hs populate most frequently the high-energy interaction mode, while in the fungal enzymes, it populates mostly the low-energy mode (although in CYP51-Cg a peak is also found in the high-energy region). The energetic difference between these two binding modes compensates almost exactly the energy difference of protein–ligand interactions in the case of CYP51-Mt, indicating that these interactions are competitive. Therefore, protein–ligand or ligand–HEME interactions cannot be used

Table 1. Interaction energies of fluconazole with the environment obtained from MD simulations.

| Energy (kcal/mol) | *Mycobacterium tuberculosis* | *Candida albicans* | *Candida glabrata* | *Homo sapiens* |
|---|---|---|---|---|
| **Ligand–environment** | −64.2 ± 8.4 | −74.4 ± 4.1 | −73.7 ± 7.6 | −67.7 ± 9.6 |
| **Ligand–water** | −12.8 ± 7.6 | −15.7 ± 3.1 | −19.3 ± 6.2 | −20.5 ± 9.2 |
| **Ligand–protein** | −32.2 ± 7.6 | −25.7 ± 3.0 | −25.5 ± 3.6 | −24.8 ± 6.1 |
| **Ligand–HEME** | −19.2 ± 4.9 | −32.9 ± 2.2 | −29.0 ± 5.0 | −22.4 ± 5.2 |

The range of interactions observed in each case is indicated by the standard deviations of the fluctuations.

Table 2. Docking results of antifungal azoles using the DockThor software and experimental affinities.

| CYP51 | T.Energy (kcal/mol) | I.Energy (kcal/mol) | RMSD (Å) | Score (kcal/mol) | $k_d$ exp |
|---|---|---|---|---|---|
| *Homo sapiens* | −0.432 | −28.036 | 1.707 | −8.100 | 30.5 μM (Warrilow et al., 2013) |
| *Mycobacterium tuberculosis* | −2.441 | −33.675 | 1.189 | −8.708 | 10 μM (Bellamine et al., 1999) |
| *Candida glabrata* | −3.775 | −32.676 | 2.410 | −8.780 | – |
| *Candida albicans* | −11.898 | −38.482 | 1.125 | −9.112 | 56 nM (Park et al., 2011; Warrilow et al., 2013) |

T.Energy corresponds to intermolecular ligand–receptor + intramolecular ligand energies, I.Energy corresponds to intermolecular ligand–receptor energy and the RMSD shown is relative to the crystallographic fluconazole conformation.

independently as indicators of the relative affinity of the ligand to the enzymes.

The total non-bonded ligand interaction energies are favorable for fungal enzymes as shown in Figure 4(A) and Table 1. The interactions of the ligand with the HEME are determinant for these differences, although they are destabilized by different mechanisms in the human or mycobacterial enzymes. In CYP51-Hs, the greater flexibility of the active site permits the entrance of water into the binding pocket, and these water molecules interact effectively with the ligand, as shown in Figure 4(D). More specifically, the ligand–water interactions display a low-energy tail in CYP51-Hs which is not present in fungal enzymes. These water molecules interact with the triazole ring of fluconazole by hydrogen bonding. These interactions compensate only in part the loss of ligand–HEME interactions relative to fungal enzymes.

Ligand–water interactions are weaker in CYP51-Mt, however (Figure 4(C)), and in conjunction with the weaker ligand–HEME interactions explain the overall lower ligand-environment energy in CYP51-Mt. As illustrated in Figure 4(E), several water molecules are present in the binding site of fungal CYP51s, and form hydrophilic interactions with fluconazole.

The interaction energies of fluconazole with the environment are, therefore, more favorable in fungal enzymes than in CYP51-Mt and CYP51-Hs, consistently with the experimentally observed affinities. This energetic advantage results from an intricate competition of ligand–protein, ligand–-water, and ligand–HEME interactions, being the ligand–HEME interactions determinant for the stronger binding to fungal enzymes.

To support the hypothesis that a structural analysis of the ligand binding poses in the crystallographic structures is sufficient to determine the relative affinities, we obtained independent affinity estimates using molecular docking (de Magalhães et al., 2014). The docking scores were −8.707 kcal/mol for CYP51-Mt, −8.100 kcal/mol for CYP51-Hs, −8.780 kcal/mol for CYP51-Cg, and −9.112 kcal/mol for CYP51-Ca (Table 2). Therefore, the docking scores are qualitatively consistent with the experimental results and with the interaction energies of the simulations: the affinity is greater for fungal enzymes, and particularly for CYP51-Ca (although only three experimental dissociation constants are available, the correlation coefficient of docking scores with the experimental $K_d$s is of 0.99). The decomposition of the energies in the docking result also suggest that part of the greater affinity to fungal enzymes is associated with the relaxation of the intramolecular energy of the ligand.

It is interesting to note that the most important docking poses are associated with the conformations of the ligand observed in the simulations for all but the CYP51-Cg ortholog. For CYP51-Ca, the optimal docking conformation displays and RMSD relative to the crystallographic conformation of only 1.125 Å, consistently with the stability of this pose observed in the simulations. For CYP51-Mt, the docking conformation is also the crystallographic one, being this conformation observed in the simulations, also it was not the most populated one (Figure 2(F)). Finally, the ligand in the human ortholog populates mostly a conformation with ∼1.7 Å deviation from the crystallographic pose (Figure 2(F)), which is consistent with the most favorable docking conformation found (Table 2).

## 4. Discussion

In this work, we have shown that the differences of affinity of fluconazole to fungal vs. mycobacterial and human CYP51 enzymes are correlated with the interaction energies of the ligand with the environment. These differences can be associated with the greater flexibility of loops of CYP51-Hs and CYP51-Mt relative to fungal orthologs. This flexibility, however, does not result in a loss of protein–ligand interactions, but in a competition of ligand interactions with the protein, the HEME group and water molecules. Effectively, fluconazole appears to interact more strongly with the protein atoms in the mycobacterial enzyme, simply because it displays an additional charged residue in the binding site (Arg96). However, these increased interactions do not correlate with the overall stabilization of the ligand in the binding pocket, because they only substitute ligand–HEME and ligand–water

interactions of fungal enzymes. The human ortholog displays less favorable ligand–environment interactions as well, consistently with the observed affinities. However, in this case, the destabilization of fluconazole binding is associated with the entrance of water in the binding pocket, resulting from its greater flexibility. These water molecules compete, as in CYP51-Mt, with ligand–HEME interactions.

The greater conformational flexibilities of the BC-loop in CYP51-Mt and CYP51-Hs result in that fluconazole deviates from the crystallographic conformation in these proteins. Also, this loop is responsible for the existence of an additional escape cavity in CYP51-Mt.

Within fungal enzymes, the most prominent interaction difference is that of residues Tyr132/Tyr141 (Figure 3(B,C)). The polar interaction of this residue in CYP51-Ca is more stable than in CYP51-Cg, at least in within the precision of the simulations performed. This difference might be explored for the development of inhibitors of greater specificity, as the CYP51-Cg variant appears to be able to accommodate slightly larger radicals at the triazole position. At the same position, the corresponding residue in CYP51-Mt is a phenylalanine which does not contact the ligand, thus reinforcing that this position is a potential site for exploring ligand structural variability.

## 5. Conclusion

MD simulations were used to explore the fluconazole binding modes of human, mycobacterial and fungal CYP51 enzymes. The human and mycobacterial enzymes are more flexible than fungal variants. CYP51-Mt displays structural fluctuations in loops that open the binding site to possible ligand entry and exit pathways that are not present in the other orthologs. This results in a ligand with greater flexibility. Nevertheless, a polar residue in the binding site of the mycobacterial ortholog leads to stronger protein–ligand interactions, in apparent contradiction with the experimental affinities. However, this substitution is compensated by interactions of the ligand with the HEME group and with water molecules, such that the overall energetics of binding favors the fungal enzymes in the order expected from the experiments. A similar phenomenon is observed for the human ortholog: increased flexibilities of the BC-loop and of the I-helix lead to a dynamic ligand binding mode in which ligand–HEME interactions are lost. Some of these interactions are substituted by interactions with water molecules, which penetrate the binding pocket of the human enzyme. These results suggest that ligands with larger hydrophobic groups will be stabilized in the binding pocket of human and mycobacterial enzymes, while smaller ligands designed to form specific polar bonds with the carboxylate groups of the HEME group should be designed to increase specificity to fungal enzymes.

## Disclosure statement

No potential conflict of interest was reported by the authors.

## Funding

The authors thank the financial support of the funding agencies Fapesp (Projects: 2010/16947-9 and 2013/08293-7) and CNPq (Project: 161305/2014-8).

## References

Balding, P. R., Porro, C. S., McLean, K. J., Sutcliffe, M. J., Maréchal, J.-D., Munro, A. W., & Visser, S. P. D. (2008). How do azoles inhibit cytochrome P450 enzymes? A density functional study. *The Journal of Physical Chemistry A*, *112*(50), 12911–12918. doi:10.1021/jp802087w

Bellamine, A., Mangla, A. T., Nes, W. D., & Waterman, M. R. (1999). Characterization and catalytic properties of the sterol 14alpha-demethylase from *Mycobacterium tuberculosis*. *Proceedings of the National Academy of Sciences of the United States of America*, *96*(16), 8937–8942. doi:10.1073/pnas.96.16.8937

Bongomin, F., Gago, S., Oladele, R. O., & Denning, D. W. (2017). Global and multi-national prevalence of fungal diseases-estimate precision. *Journal of Fungi (Fungi)*, *3*(4), pii: E57. doi:10.3390/jof3040057

Brown, G. D., Denning, D. W., & Levitz, S. M. (2012). Tackling human fungal infections. *Science (New York, N.Y.)*, *336*(6082), 647. doi:10.1126/science.1222236

Castanheira, M., Messer, S. A., Jones, R. N., Farrell, D. J., & Pfaller, M. A. (2014). Activity of echinocandins and triazoles against a contemporary (2012) worldwide collection of yeast and moulds collected from invasive infections. *International Journal of Antimicrobial Agents*, *44*(4), 320–326. doi:10.1016/j.ijantimicag.2014.06.007

Choi, J., & Roush, W. (2016). Structure based design of CYP51 inhibitors. *Current Topics in Medicinal Chemistry*, *17*(1), 30–39. doi:10.2174/1568026616666160719164933

de Magalhães, C. S., Almeida, D. M., Barbosa, H. J. C., & Dardenne, L. E. (2014). A dynamic niching genetic algorithm strategy for docking highly flexible ligands. *Information Sciences*, *289*, 206–224. doi:10.1016/j.ins.2014.08.002

de Magalhães, C. S., Barbosa, H. J. C., & Dardenne, L. E. (2004). Selection-insertion schemes in genetic algorithms for the flexible ligand docking problem. In K. Deb (Ed.), Lecture notes in computer science (Vol. 3102, pp. 368–379). Berlin, Heidelberg: Springer.

Doğan, İS., Saraç, S., Sari, S., Kart, D., Eşsiz Gökhan, Ş., Vural, İ., & Dalkara, S. (2017). New azole derivatives showing antimicrobial effects and their mechanism of antifungal activity by molecular modeling studies. *European Journal of Medicinal Chemistry*, *130*, 124–138. doi:10.1016/j.ejmech.2017.02.035

Essmann, U., Perera, L., Berkowitz, M. L., Darden, T., Lee, H., & Pedersen, L. G. (1995). A smooth particle mesh Ewald method. *The Journal of Chemical Physics*, *103*(19), 8577–8593. doi:10.1063/1.470117

Gao, P., Cui, Y.-L., & Wu, R.-L. (2018). Molecular dynamic modeling of CYP51B in complex with azole inhibitors. *Journal of Biomolecular Structure & Dynamics*, *36*(6), 1511–1519. doi:10.1080/07391102.2017.1328315

Gordon, J. C., Myers, J. B., Folta, T., Shoja, V., Heath, L. S., & Onufriev, A. (2005). H: A server for estimating pKas and adding missing hydrogens to macromolecules. *Nucleic Acids Research*, *33*(Web Server), W368–W371. doi:10.1093/nar/gki464

Hargrove, T., Wawrzak, Z., & Lepesheva, G. (2017). Crystal structure of sterol 14-alpha demethylase (CYP51) from Candida albicans in complex with the tetrazole-based antifungal drug candidate VT1161 (VT1). https://doi.org/10.2210/pdb5tz1/pdb

Hargrove, T. Y., Friggeri, L., Wawrzak, Z., Qi, A., Hoekstra, W. J., Schotzinger, R. J., … Lepesheva, G. I. (2017). Structural analyses of *Candida albicans* sterol 14α-demethylase complexed with azole drugs address the molecular basis of azole-mediated inhibition of fungal sterol biosynthesis. *Journal of Biological Chemistry*, *292*(16), 6728–6743. doi:10.1074/jbc.M117.778308

Hargrove, T. Y., Wawrzak, Z., Lamb, D. C., Guengerich, F. P., & Lepesheva, G. I. (2015). Structure-functional characterization of cytochrome P450 sterol 14α-demethylase (CYP51B) from *Aspergillus fumigatus* and molecular basis for the development of antifungal drugs. *Journal of Biological Chemistry*, *290*(39), 23916–23934. doi:10.1074/jbc.M115.677310

Huang, J., & MacKerell, A. D. Jr.(2013). CHARMM36 all-atom additive protein force field: Validation based on comparison to NMR data. *Journal of Computational Chemistry*, *34*(25), 2135–2145. doi:10.1002/jcc.23354

Humphrey, W., Dalke, A., & Schulten, K. (1996). VMD: Visual molecular dynamics. *Journal of Molecular Graphics*, *14*(1), 33–38. 27–28. doi:10.1016/0263-7855(96)00018-5

Jacob K., S., Ganguly, S., Kumar, P., Poddar, R., & Kumar, A. (2017). Homology model, molecular dynamics simulation and novel pyrazole analogs design of *Candida albicans* CYP450 lanosterol 14 α-demethylase, a target enzyme for antifungal therapy. *Journal of Biomolecular Structure & Dynamics*, *35*(7), 1446–1463. doi:10.1080/07391102.2016.1185380

Jorgensen, W. L., Chandrasekhar, J., Madura, J. D., Impey, R. W., & Klein, M. L. (1983). Comparison of simple potential functions for simulating liquid water. *The Journal of Chemical Physics*, *79*(2), 926–935. doi:10.1063/1.445869

Kalé, L., Skeel, R., Bhandarkar, M., Brunner, R., Gursoy, A., Krawetz, N., … Schulten, K. (1999). NAMD2: Greater scalability for parallel molecular dynamics. *Journal of Computational Physics*, *151*(1), 283–312. doi:10.1006/jcph.1999.6201

Keighobadi, M., Emami, S., Lagzian, M., Fakhar, M., Rafiei, A., & Valadan, R. (2018). Molecular modeling and structural stability of wild-type and mutant CYP51 from *Leishmania major*: In vitro and in silico analysis of a laboratory strain. *Molecules*, *23*(3), pii:E696. doi:10.3390/molecules23030696

Kenaan, C., Zhang, H., Shea, E. V., & Hollenberg, P. F. (2011). Uncovering the role of hydrophobic residues in cytochrome P450-cytochrome P450 reductase interactions. *Biochemistry*, *50*(19), 3957–3967. doi:10.1021/bi1020748

Kontoyianni, M., & Lacy, B. (2018). Toward computational understanding of molecular recognition in the human metabolizing cytochrome P450s. *Current Medicinal Chemistry*, *25*(28), 3353–3373. doi:10.2174/0929867325666180226104126

Lepesheva, G. I., & Waterman, M. R. (2007). Sterol 14alpha-demethylase cytochrome P450 (CYP51), a P450 in all biological kingdoms. *Biochimica et Biophysica Acta*, *1770*(3), 467–477. doi:10.1016/j.bbagen.2006.07.018

Lepesheva, G. I., & Waterman, M. R. (2011). Structural basis for conservation in the CYP51 family. *Biochimica et Biophysica Acta*, *1814*(1), 88–93. doi:10.1016/j.bbapap.2010.06.006

Lupetti, A., Danesi, R., Campa, M., Del Tacca, M., & Kelly, S. (2002). Molecular basis of resistance to azole antifungals. *Trends in Molecular Medicine*, *8*(2), 76–81.

MacKerell, A. D., Bashford, D., Bellott, M., Dunbrack, R. L., Evanseck, J. D., Field, M. J., … Karplus, M. (1998). All-atom empirical potential for molecular modeling and dynamics studies of proteins. *The Journal of Physical Chemistry B*, *102*(18), 3586–3616. doi:10.1021/jp973084f

Marichal, P., Gorrens, J., Laurijssens, L., Vermuyten, K., Van Hove, C., Le Jeune, L., … Vanden Bossche, H. (1999). Accumulation of 3-ketosteroids induced by itraconazole in azole-resistant clinical *Candida albicans* isolates. *Antimicrobial Agents and Chemotherapy*, *43*(11), 2663–2670. doi:10.1128/AAC.43.11.2663

Martínez, L. (2015). Automatic identification of mobile and rigid substructures in molecular dynamics simulations and fractional structural fluctuation analysis. *PLoS One*, *10*(3), e0119264. doi:10.1371/journal.pone.0119264

Martínez, L. (2017). MDAnalysis (Version 17.224). Retrieved from http://leandro.iqm.unicamp.br/mdanalysis

Mayne, C. G., Saam, J., Schulten, K., Tajkhorshid, E., & Gumbart, J. C. (2013). Rapid parameterization of small molecules using the Force Field Toolkit. *Journal of Computational Chemistry*, *34*(32), 2757–2770. doi:10.1002/jcc.23422

McLean, K. J., Clift, D., Lewis, D. G., Sabri, M., Balding, P. R., Sutcliffe, M. J., … Munro, A. W. (2006). The preponderance of P450s in the *Mycobacterium tuberculosis* genome. *Trends in Microbiology*, *14*(5), 220–228. doi:10.1016/j.tim.2006.03.002

Park, H.-G., Lee, I.-S., Chun, Y.-J., Yun, C.-H., Johnston, J. B., Montellano, P. R. O., de, & … Im, D. (2011). Heterologous expression and characterization of the sterol 14α-demethylase CYP51F1 from *Candida albicans*. *Archives of Biochemistry and Biophysics*, *509*(1), 9–15. doi:10.1016/j.abb.2011.02.002

Pfaller, M. A., Andes, D. R., Diekema, D. J., Horn, D. L., Reboli, A. C., Rotstein, C., … Azie, N. E. (2014). Epidemiology and outcomes of invasive candidiasis due to non-albicans species of *Candida* in 2,496 patients: Data from the Prospective Antifungal Therapy (PATH) registry 2004-2008. *PLoS One*, *9*(7), e101510. doi:10.1371/journal.pone.0101510

Podust, L. M., Poulos, T. L., & Waterman, M. R. (2001). Crystal structure of cytochrome P450 14alpha -sterol demethylase (CYP51) from *Mycobacterium tuberculosis* in complex with azole inhibitors. *Proceedings of the National Academy of Sciences of the United States of America*, *98*(6), 3068–3073. doi:10.1073/pnas.061562898

Robert, X., & Gouet, P. (2014). Deciphering key features in protein structures with the new ENDscript server. *Nucleic Acids Research*, *42*(W1, Web Server issue), W320–W324. doi:10.1093/nar/gku316

Sagatova, A. A., Keniya, M. V., Wilson, R. K., Monk, B. C., & Tyndall, J. D. A. (2015). Structural insights into binding of the antifungal drug fluconazole to *Saccharomyces cerevisiae* lanosterol 14α-demethylase. *Antimicrobial Agents and Chemotherapy*, *59*(8), 4982–4989. doi:10.1128/AAC.00925-15

Schrödinger, L. C. C. (2015). The PyMOL Molecular Graphics System (Version 2.0).

Shapiro, R. S., Robbins, N., & Cowen, L. E. (2011). Regulatory circuitry governing fungal development, drug resistance, and disease. *Microbiology and Molecular Biology Reviews: MMBR*, *75*(2), 213–267. doi:10.1128/MMBR.00045-10

Sheng, C., Chen, S., Ji, H., Dong, G., Che, X., Wang, W., … Zhang, W. (2010). Evolutionary trace analysis of CYP51 family: Implication for site-directed mutagenesis and novel antifungal drug design. *Journal of Molecular Modeling*, *16*(2), 279–284. doi:10.1007/s00894-009-0527-9

Sievers, F., Wilm, A., Dineen, D., Gibson, T. J., Karplus, K., Li, W., … Higgins, D. G. (2011). Fast, scalable generation of high-quality protein multiple sequence alignments using clustal omega. *Molecular Systems Biology*, *7*(1), 539. doi:10.1038/msb.2011.75

Strushkevich, N., Usanov, S. A., & Park, H.-W. (2010). Structural basis of human CYP51 inhibition by antifungal azoles. *Journal of Molecular Biology*, *397*(4), 1067–1078. doi:10.1016/j.jmb.2010.01.075

Strushkevich, N. V., Harnastai, I. N., & Usanov, S. A. (2010). Mechanism of steroidogenic electron transport: Role of conserved Glu429 in destabilization of CYP11A1-adrenodoxin complex. *Biochemistry (Moscow)*, *75*(5), 570–578. doi:10.1134/S0006297910050056

Swope, W. C., Andersen, H. C., Berens, P. H., & Wilson, K. R. (1982). A computer simulation method for the calculation of equilibrium constants for the formation of physical clusters of molecules: Application to small water clusters. *The Journal of Chemical Physics*, *76*(1), 637–649. doi:10.1063/1.442716

Vanommeslaeghe, K., Hatcher, E., Acharya, C., Kundu, S., Zhong, S., Shim, J., … Mackerell, A. D. Jr.(2010). CHARMM general force field: A force field for drug-like molecules compatible with the CHARMM all-atom additive biological force fields. *Journal of Computational Chemistry*, *31*(4), 671–690. doi:10.1002/jcc.21367

Vanommeslaeghe, K., Raman, E. P., & MacKerell, A. D. Jr. (2012). Automation of the CHARMM General Force Field (CGenFF) II: Assignment of bonded parameters and partial atomic charges. *Journal of Chemical Information and Modeling*, *52*(12), 3155–3168. doi:10.1021/ci3003649

Vijayakumar, S., & Das, P. (2019). Structural, molecular motions, and free-energy landscape of *Leishmania* sterol-14α-demethylase wild type and drug resistant mutant: A comparative molecular dynamics study. *Journal of Biomolecular Structure & Dynamics*, *37*(6), 1477–1493. doi:10.1080/07391102.2018.1461135

Warrilow, A. G., Parker, J. E., Kelly, D. E., & Kelly, S. L. (2013). Azole affinity of sterol 14α-demethylase (CYP51) enzymes from *Candida albicans* and *Homo sapiens*. *Antimicrobial Agents and Chemotherapy*, *57*(3), 1352–1360. doi:10.1128/AAC.02067-12

White, T. C., Marr, K. A., & Bowden, R. A. (1998). Clinical, cellular, and molecular factors that contribute to antifungal drug resistance. *Clinical Microbiology Reviews*, *11*(2), 382–402. doi:10.1128/CMR.11.2.382